Neutron matter at finite temperature

L. Tolos[1], B. Friman[2] and A. Schwenk[3]

[1]*FIAS, J.W. Goethe Universität, Ruth-Moufang-Str. 1,*
D-60438 Frankfurt am Main, Germany
[2]*GSI, Planckstr. 1, D-64291 Darmstadt, Germany*
[3]*TRIUMF, 4004 Wesbrook Mall, Vancouver, BC, Canada, V6T 2A3*

Abstract

We calculate the neutron matter equation of state at finite temperature based on low-momentum two- and three-nucleon interactions. The free energy is obtained from a loop expansion around the Hartree-Fock energy, including contributions from normal and anomalous diagrams. We focus on densities below saturation density with temperatures $T \leqslant 10\,\text{MeV}$ and compare our results to the model-independent virial equation of state and to variational calculations. Good agreement with the virial equation of state is found at low density. We provide simple estimates for the theoretical error, important for extrapolations to astrophysical conditions.

1 Introduction

The nuclear equation of state plays a central role in astrophysics, for problems ranging from the structure of neutron stars [1], neutron star mergers [2] to core-collapse supernovae [3,4]. Astrophysical applications probe the equation of state at the extremes of isospin and temperature: The mass of a neutron star depends mainly on the equation of state of neutron matter up to densities $\rho \sim 4\rho_0$ [5], where $\rho_0 = 0.16\,\text{fm}^{-3}$ is the saturation density of symmetric nuclear matter, while supernova explosions are most sensitive to the properties of nucleonic matter at subnuclear densities and MeV temperatures [3]. For many regimes of interest, the equation of state has to be extrapolated from the conditions reached with existing and upcoming experimental facilities. Therefore, reliable theoretical input is needed. In this paper, we present a study of neutron matter at finite temperature, as part of a program to improve the nuclear equation of state input for astrophysics.

Email addresses: `tolos@fias.uni-frankfurt.de` (L. Tolos), `b.friman@gsi.de` (B. Friman), `schwenk@triumf.ca` (A. Schwenk).

Conventional nucleon-nucleon (NN) interactions are nonperturbative as a result of several sources. First, there is a strong short-range repulsion, which leads to bound states of the "flipped" potential λV_{NN} for small, negative λ. This implies that $\lambda = 1$ is far outside the radius of convergence. Consequently, at least the summation of particle-particle ladder diagrams is required [6]. Second, the tensor force, which is singular at short distances, requires iteration in the triplet channels [7,8]. Finally, there are physical bound and nearly-bound states in the S-waves, which render the perturbative Born series divergent. Recently, it was shown that the first two sources of nonperturbative behavior depend on the choice of NN interaction, and can be removed by evolving nuclear forces to low-momentum interactions $V_{\text{low }k}$ [9,10,11,12] with cutoffs around $2\,\text{fm}^{-1}$ [13,14]. An important additional advantage is that the corresponding leading-order three-nucleon (3N) interactions from chiral effective field theory (EFT) become perturbative in light nuclei for cutoffs $\Lambda \lesssim 2\,\text{fm}^{-1}$ [15].

At sufficient density ($\rho \gtrsim 0.01\rho_0$ [16] in nuclear matter), Pauli blocking eliminates the shallow bound states, and thus the particle-particle channel becomes perturbative [13]. Consequently, the Hartree-Fock (HF) approximation is a good starting point for low-momentum NN and 3N interactions, and perturbation theory (in the sense of a loop expansion) around the HF energy becomes tractable. The perturbative character is due to a combination of Pauli blocking and an appreciable effective range (see also Ref. [17]). The 3N interaction is essential for nuclear matter saturation [13], while the contributions to the potential energy remain compatible with EFT power-counting estimates. Furthermore, the equation of state becomes significantly less cutoff dependent with the inclusion of the dominant second-order contributions. In this paper, we extend the investigation of Ref. [13] to neutron matter at subsaturation densities, $\rho < \rho_0$, and generalize the perturbative approach to finite temperature.

Based on the work of Kohn, Luttinger and Ward [18,19], at finite temperature the loop expansion around the HF free energy can be realized by the perturbative expansion of the free energy. In this paper, we include the first-order NN and 3N contributions, as well as anomalous and normal second-order diagrams with NN interactions. We defer 3N contributions beyond the HF level and higher-order corrections to future work. The pressure, entropy and energy are calculated using standard thermodynamic relations. Since low-momentum interactions are energy independent, the Matsubara sums can be carried out analytically.

Low-momentum interactions $V_{\text{low }k}$ and the corresponding 3N forces are defined by sharp or smooth regulators with a variable momentum cutoff Λ. Varying the cutoff is a powerful tool to estimate the theoretical errors due to neglected higher-order many-body interactions and to assess the completeness of the calculations. We use the cutoff dependence to provide simple error estimates,

and find that the cutoff dependence is reduced significantly, when second-order contributions are included. The possibility of estimating theoretical errors is an important step towards reliable extrapolations to astrophysical conditions. Finally, we compare our results to the virial equation of state [20,21] and to variational calculations [22]. The low-density behavior is in good agreement with the virial equation of state. Our results for the energy per particle (see Fig. 5) highlight the importance of a correct finite-temperature treatment of second and higher-order correlations.

This paper is organized as follows. In Sect. 2, we discuss the perturbative expansion at finite temperature and give the expressions for the evaluated diagrams. Our results for the free energy, pressure, entropy and energy are presented in Sect. 3. We conclude and give an outlook in Sect. 4.

2   Loop expansion at finite temperature

We consider the perturbative expansion of the grand-canonical potential,

$$\Omega(\mu, T, V) = -\beta \ln \mathcal{Z}(\mu, T, V) \,, \tag{1}$$

where $\mathcal{Z}(\mu, T, V)$ denotes the partition function of the interacting Fermi system, μ is the chemical potential, $\beta = 1/T$ the inverse temperature and V the volume. We include the first-order NN and 3N contributions, $\Omega_{1,\mathrm{NN}}$ and $\Omega_{1,\mathrm{3N}}$, as well as the second-order anomalous and normal contributions with NN interactions, $\Omega_{2,\mathrm{a}}$ and $\Omega_{2,\mathrm{n}}$. The grand-canonical potential is then given by

$$\begin{aligned} \Omega &= \Omega_0 + \Omega_1 + \Omega_2 + \dots \\ &= \Omega_0 + (\Omega_{1,\mathrm{NN}} + \Omega_{1,\mathrm{3N}}) + (\Omega_{2,\mathrm{a}} + \Omega_{2,\mathrm{n}}) + \dots \,, \end{aligned} \tag{2}$$

where terms of the same order are enclosed in brackets, and Ω_0 is the grand-canonical potential of the non-interacting system,

$$\frac{\Omega_0}{V} = -2\,T \int \frac{d\mathbf{k}}{(2\pi)^3} \, \ln\!\Big(1 + e^{-\beta(\epsilon_k - \mu)}\Big) = -2 \int \frac{d\mathbf{k}}{(2\pi)^3} \, \frac{k^2}{3m} \, n_k \,. \tag{3}$$

Here, $\epsilon_k = k^2/(2m)$ is the free single-particle energy, with m the nucleon mass, and $n_k = 1/[e^{\beta(\epsilon_k - \mu)} + 1]$ is the Fermi-Dirac distribution function. The different contributions are depicted diagrammatically in Fig. 1.

The loop expansion around the HF energy is realized by the perturbative expansion of the free energy $F(N, T, V)$, which is obtained by a Legendre transformation of the grand-canonical potential with respect to the chemical potential,
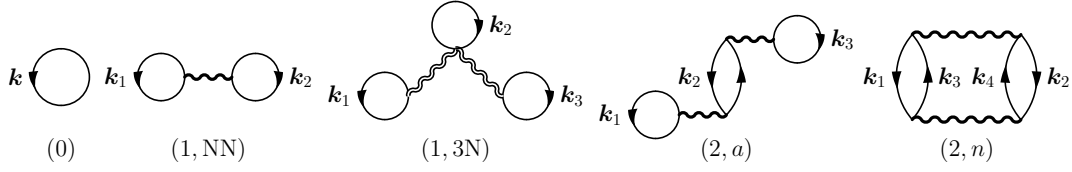
$$F(N, T, V) = \Omega(\mu, T, V) + \mu\,N \,. \tag{4}$$

Fig. 1. Non-interacting (0); first-order NN $(1, \text{NN})$ and 3N $(1, 3\text{N})$; second-order anomalous $(2, \text{a})$ and normal $(2, \text{n})$ contributions to the grand-canonical potential $\Omega(\mu, T, V)$. The wiggly and double-wiggly lines denote antisymmetrized low-momentum NN and 3N interactions, respectively.

The mean particle number $N \equiv \langle N \rangle$ is given by

$$N(\mu, T, V) = -\frac{\partial \Omega}{\partial \mu}\bigg|_{T,V} = -\frac{\partial \Omega_0}{\partial \mu}\bigg|_{T,V} - \frac{\partial \Omega_1}{\partial \mu}\bigg|_{T,V} - \frac{\partial \Omega_2}{\partial \mu}\bigg|_{T,V} - \dots . \quad (5)$$

In order to invert Eq. (5) for the chemical potential $\mu(N, T, V)$, we follow the treatment of Kohn and Luttinger [18] and expand μ to the same order

$$\mu = \mu_0 + \mu_1 + \mu_2 + \dots , \quad (6)$$

where the particle number is counted as order zero. The lowest order term μ_0 is the chemical potential of a non-interacting system with the same density $\rho = N/V$ as the interacting system.

Expanding each term on the right-hand side of Eq. (5) around $\mu = \mu_0$ and solving for the chemical potential order by order leads to

$$N = -\frac{\partial \Omega_0}{\partial \mu}\bigg|_{\mu_0} \quad \text{and} \quad \mu_1 = -\frac{\partial \Omega_1/\partial \mu}{\partial^2 \Omega_0/\partial \mu^2}\bigg|_{\mu_0} , \quad (7)$$

and correspondingly for the free energy

$$F = \Omega_0(\mu_0) + (\mu_1 + \mu_2) \frac{\partial \Omega_0}{\partial \mu}\bigg|_{\mu_0} + \frac{1}{2} \mu_1^2 \frac{\partial^2 \Omega_0}{\partial \mu^2}\bigg|_{\mu_0} + \Omega_1(\mu_0) + \mu_1 \frac{\partial \Omega_1}{\partial \mu}\bigg|_{\mu_0} + \Omega_2(\mu_0)$$

$$+ \mu_0 N + (\mu_1 + \mu_2)N + \dots . \quad (8)$$

Using Eq. (7), we find

$$F(N) = F_0(N) + \Omega_1(\mu_0) + \Omega_2(\mu_0) - \frac{1}{2} \frac{(\partial \Omega_1/\partial \mu)^2}{\partial^2 \Omega_0/\partial \mu^2}\bigg|_{\mu_0} , \quad (9)$$

where $F_0(N) = \Omega_0(\mu_0) + \mu_0 N$ is the free energy of the non-interacting system. Since we neglect the contribution of 3N interactions in second-order diagrams, we consistently keep only the first-order NN part $\Omega_{1,\text{NN}}$ in the term

4

$(\partial \Omega_1 / \partial \mu)^2|_{\mu_0}$. Consequently, we have

$$F(N) = F_0(N) + \Omega_1(\mu_0) + \Omega_{2,\mathrm{n}}(\mu_0) + \left[\Omega_{2,\mathrm{a}}(\mu_0) - \frac{1}{2} \frac{(\partial \Omega_{1,\mathrm{NN}}/\partial \mu)^2}{\partial^2 \Omega_0 / \partial \mu^2} \Bigg|_{\mu_0} \right]. \quad (10)$$

According to the Kohn-Luttinger-Ward theorem [18,19], the term in the square brackets vanishes at $T = 0$ for isotropic, normal Fermi systems, since the anomalous diagram cancels against the contribution induced in $\Omega_{1,\mathrm{NN}}$ by the shift of the chemical potential. Thus, the above expansion ensures that the $T \to 0$ limit is correctly reproduced.

In the $T \to 0$ limit $\mu_0 = \epsilon_\mathrm{F} = k_\mathrm{F}^2/(2m)$, where k_F is the Fermi momentum, and the ground state energy of the interacting system is given by $F \to E = E_0 + \Omega_1(\epsilon_\mathrm{F}) + \Omega_{2,\mathrm{n}}(\epsilon_\mathrm{F}) + \ldots$. For a momentum-independent contact interaction, the square bracket in Eq. (10) vanishes at all temperatures, since in this case the HF self-energy is momentum independent. Consequently, the thermodynamic potential derived from the free energy Eq. (10) corresponds exactly to the loop expansion around the HF energy. For finite-range interactions, the HF self-energy is momentum dependent, and the cancellation is exact only in the zero-temperature limit. At finite temperature, the momentum dependence of the HF self-energy is therefore treated perturbatively.

The pressure, entropy and energy follow from the free energy using standard thermodynamic relations. The entropy per particle S/N is given by

$$\frac{S}{N} = -\frac{\partial (F/N)}{\partial T}\Bigg|_{N,V} = -\frac{\partial (f/\rho)}{\partial T}\Bigg|_{N,V}, \quad (11)$$

where $f = F/V$ is the free-energy density. The chemical potential is given by $\mu = \partial_N F|_{T,V}$ and the pressure P follows from

$$P = \mu \rho - f = \frac{N^2}{V} \frac{\partial (F/N)}{\partial N}\Bigg|_T = \rho^2 \frac{\partial (f/\rho)}{\partial \rho}\Bigg|_T. \quad (12)$$

Finally, the energy per particle is obtained from $E/N = F/N + T(S/N)$.

2.1 Hartree-Fock NN and 3N diagrams

The first-order $V_{\mathrm{low}\,k}$ contribution, (1,NN) in Fig. 1, is given by

$$\frac{\Omega_{1,\mathrm{NN}}}{V} = \frac{1}{2} \mathrm{Tr}_{\sigma_1,\sigma_2} \int \frac{d\mathbf{k}_1}{(2\pi)^3} \int \frac{d\mathbf{k}_2}{(2\pi)^3} \, n_{k_1} \, n_{k_2} \, \langle 12 \, | \, V_{\mathrm{low}\,k} \, (1 - P_{12}) \, | \, 12 \rangle, \quad (13)$$

where the trace is over the spins of the two neutrons and P_{12} denotes the exchange operator for spin and momenta of nucleons 1 and 2. Note that the

momentum-conserving delta function is not included in the NN matrix elements.

In neutron matter, the effect of 3N interactions is expected to be smaller than in symmetric matter, since the Pauli principle prevents three neutrons from interacting in a relative S-state. In the evaluation of the first-order 3N diagram, $(1,3N)$ in Fig. 1, we follow Ref. [13]. At the HF level only the c_1 and c_3 terms of the long-range 2π-exchange part contribute:

$$
\frac{\Omega_{1,3N}}{V} = \frac{g_A^2}{4f_\pi^2} \int \frac{d\mathbf{k}_1}{(2\pi)^3} \int \frac{d\mathbf{k}_2}{(2\pi)^3} \int \frac{d\mathbf{k}_3}{(2\pi)^3} \, n_{k_1} \, n_{k_2} \, n_{k_3} \, f_R^2(p,q)
$$
$$
\times \left[-\frac{4c_1 m_\pi^2}{f_\pi^2} \left(2 \frac{\mathbf{k}_{12} \cdot \mathbf{k}_{23}}{(k_{12}^2 + m_\pi^2)(k_{23}^2 + m_\pi^2)} + 2 \frac{k_{12}^2}{(k_{12}^2 + m_\pi^2)^2} \right) \right.
$$
$$
\left. + \frac{2c_3}{f_\pi^2} \left(2 \frac{(\mathbf{k}_{12} \cdot \mathbf{k}_{23})^2}{(k_{12}^2 + m_\pi^2)(k_{23}^2 + m_\pi^2)} - 2 \frac{k_{12}^4}{(k_{12}^2 + m_\pi^2)^2} \right) \right], \tag{14}
$$

where $g_A = 1.29$, $f_\pi = 92.4\,\text{MeV}$, $m_\pi = 138.04\,\text{MeV}$ and $\mathbf{k}_{ij} = \mathbf{k}_i - \mathbf{k}_j$. As discussed in Ref. [15], we use the c_i constants extracted by the Nijmegen group in a partial wave analysis with chiral 2π-exchange [23]: $c_1 = -0.76\,\text{GeV}^{-1}$ and $c_3 = -4.78\,\text{GeV}^{-1}$, where the dominant contribution is due to c_3. The low-energy constants c_i are within errors consistent with the determination from πN data [24], but at present c_3 has a large theoretical uncertainty $\approx 25\%$, which is not included in our error bands (see however Fig. 6). For the 3N contribution, we have the regulator [15]

$$
f_R(p,q) = \exp\left[-\left(\frac{p^2 + 3q^2/4}{\Lambda^2} \right)^4 \right] \tag{15}
$$

where p and q are Jacobi momenta. Based on the nuclear matter results of Ref. [13], we expect that the c_3 term is repulsive and the dominant part of the 3N contribution, and that the c_1 term is small.

2.2 Second-order anomalous and normal diagrams

The second-order anomalous contribution, $(2,a)$ in Fig. 1, is given by

$$
\frac{\Omega_{2,a}}{V} = -\frac{1}{2T} \left(\prod_{i=1}^{3} \text{Tr}_{\sigma_i} \int \frac{d\mathbf{k}_i}{(2\pi)^3} \right) n_{k_1} \, n_{k_2} \, (1 - n_{k_2}) \, n_{k_3}
$$
$$
\times \langle 12 \,|\, V_{\text{low}\,k} \, (1 - P_{12}) \,|\, 12 \rangle \langle 23 \,|\, V_{\text{low}\,k} \, (1 - P_{12}) \,|\, 23 \rangle . \tag{16}
$$

We note that in the HF approximation, all tadpole self-energy insertions, including the anomalous diagram $(2,a)$, are included in the HF mean-field.

6

Hence, in a loop expansion around the HF solution, the first anomalous diagrams are of fourth order and involve two second-order self-energy insertions in place of the tadpoles in diagram (2,a). As discussed above, the present approach is equivalent to a loop expansion around the HF energy for a momentum-independent contact interaction. It follows that the contribution from the square bracket in Eq. (10) is small, although the anomalous diagram (2,a) is significant. The reasons are: First, at zero temperature the square bracket vanishes, and therefore the contribution is small at low temperatures, and second, at finite temperature it is non zero only due to the weak momentum dependence of the HF self-energy in neutron matter.

The second-order normal diagram, (2,n) in Fig. 1, reads

$$
\frac{\Omega_{2,\mathrm{n}}}{V} = -\frac{1}{8} \left(\prod_{i=1}^{4} \mathrm{Tr}_{\sigma_i} \int \frac{d\mathbf{k}_i}{(2\pi)^3} \right) (2\pi)^3 \delta(\mathbf{k}_1 + \mathbf{k}_2 - \mathbf{k}_3 - \mathbf{k}_4)
$$

$$
\times \frac{n_{k_1} n_{k_2} (1 - n_{k_3})(1 - n_{k_4}) - (1 - n_{k_1})(1 - n_{k_2}) n_{k_3} n_{k_4}}{\epsilon_{k_3} + \epsilon_{k_4} - \epsilon_{k_1} - \epsilon_{k_2}}
$$

$$
\times \left| \langle 12 \,|\, V_{\mathrm{low}\,k} \,(1 - P_{12}) \,|\, 34 \rangle \right|^2 . \tag{17}
$$

Expanding in partial waves and performing the spin traces, we find

$$
\sum_{S, M_S, M_S'} \left| \langle \mathbf{k}\, S M_S \,|\, V_{\mathrm{low}\,k} \,(1 - P_{12}) \,|\, \mathbf{k}'\, S M_S' \rangle \right|^2
$$

$$
= \sum_L P_L(\cos\theta_{\mathbf{k},\mathbf{k}'}) \sum_{J, l, l', S} \sum_{\widetilde{J}, \widetilde{l}, \widetilde{l}'} (4\pi)^2 \, i^{(l - l' + \widetilde{l} - \widetilde{l}')}
$$

$$
\times \langle k \,|\, V_{\mathrm{low}\,k}^{J l' l S} \,|\, k' \rangle \langle k' \,|\, V_{\mathrm{low}\,k}^{\widetilde{J} \widetilde{l}' \widetilde{l} S} \,|\, k \rangle \left(1 - (-1)^{l+S+1}\right) \left(1 - (-1)^{\widetilde{l}+S+1}\right)
$$

$$
\times \sqrt{(2l+1)(2l'+1)(2\widetilde{l}+1)(2\widetilde{l}'+1)} \,(2J+1)(2\widetilde{J}+1)\,(-1)^{\widetilde{l}+l'+L}
$$

$$
\times \left(l\,0\,\widetilde{l}'\,0 \,|\, L\,0 \right) \left(l'\,0\,\widetilde{l}\,0 \,|\, L\,0 \right) \begin{Bmatrix} l & S & J \\ \widetilde{J} & L & \widetilde{l}' \end{Bmatrix} \begin{Bmatrix} J & S & l' \\ \widetilde{l} & L & \widetilde{J} \end{Bmatrix}, \tag{18}
$$

where $\theta_{\mathbf{k},\mathbf{k}'}$ is the angle between relative momenta $\mathbf{k} = (\mathbf{k}_1 - \mathbf{k}_2)/2$ and $\mathbf{k}' = (\mathbf{k}_3 - \mathbf{k}_4)/2$. Keeping only $L = 0$ in Eq. (18) would result in an angle average of the Pauli-blocking operator, but all $L \leqslant 6$ are included in our results.
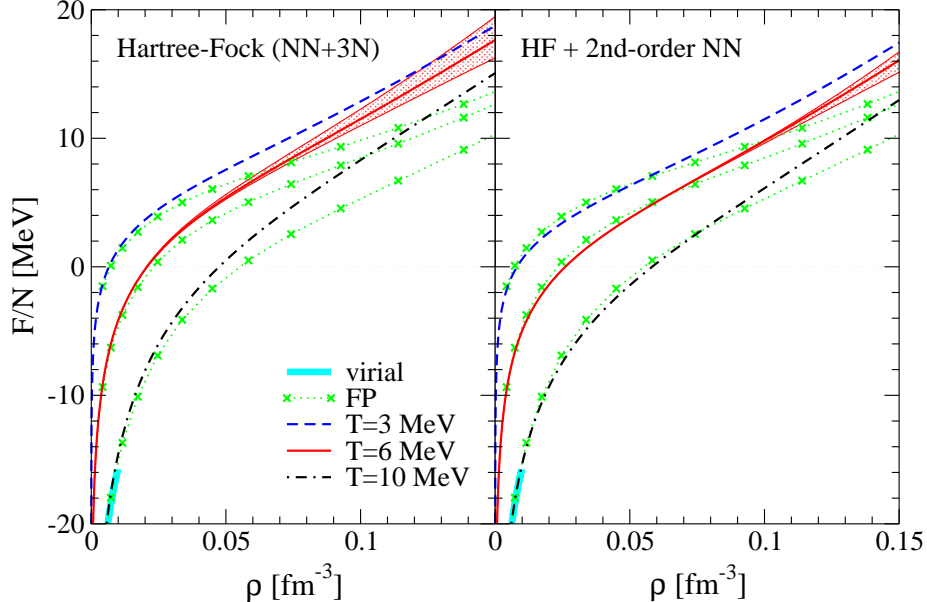
Fig. 2. The free energy per particle F/N as a function of density ρ. The left figure gives the first-order NN and 3N contributions with a free single-particle spectrum. Second-order anomalous and normal NN contributions are included in the right figure. Our results are compared to the virial equation of state (virial) [21] and to the variational calculations of Friedman and Pandharipande (FP) [22]. The virial curve ends where the fugacity $z = e^{\mu/T} = 0.5$.

3 Results

We compute the different contributions to the free energy using the adaptive Monte Carlo integration routine Vegas [25]. Our results[1] for the free energy per particle are shown in Fig. 2 for temperatures $T = 3\,\text{MeV}, 6\,\text{MeV}$ and $10\,\text{MeV}$, where the low-momentum interaction $V_{\text{low}\,k}$ is obtained from the Argonne v_{18} potential [27] for a cutoff $\Lambda = 2.1\,\text{fm}^{-1}$. The cutoff dependence of the free energy can be used to provide lower limits for the theoretical uncertainty in the calculation, since the result should be cutoff independent when all relevant contributions are included. For the $T = 6\,\text{MeV}$ results, we provide error estimates by varying the cutoff over the range $\Lambda = 1.9\,\text{fm}^{-1}$ (lower curve) to $\Lambda = 2.5\,\text{fm}^{-1}$ (upper curve). The cutoff dependence of the $T = 3\,\text{MeV}$ and $10\,\text{MeV}$ results here and in the following is of similar size. As expected, the error grows with increasing density. Moreover, we observe that the equation of state becomes significantly less cutoff dependent with the inclusion of the second-order NN contributions.

In Fig. 2, we also compare our results for the free energy to the model-independent virial equation of state [21] and to the variational calculations

---

[1] We take the opportunity to correct an error in Ref. [26], where the 3N contribution had an incorrect factor in the numerical computation.
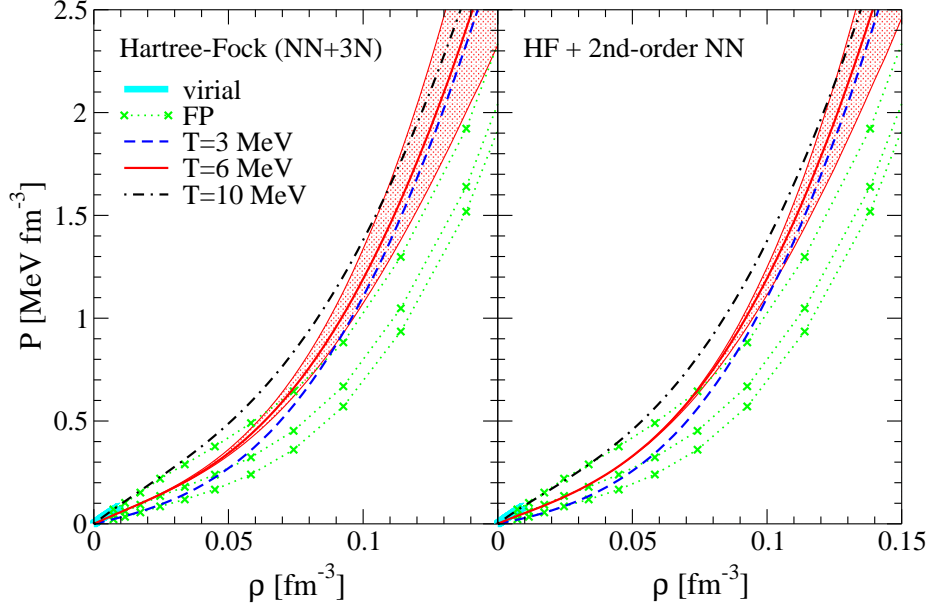
Fig. 3. The pressure P as a function of density ρ to first and second order (for details see Fig. 2). The different-temperature FP results are best identified at low density by comparison with our results.

of Friedman and Pandharipande [22] (FP, based on the Argonne v_{14} and a 3N potential). The virial expansion provides a benchmark for low densities and high temperatures, where the interparticle separation is large compared to the thermal wavelength. We find a very good agreement with the virial free energy. Including second-order NN contributions to the HF free energy brings our results closer to the FP calculations, but this trend is opposite for other thermodynamic potentials, see for instance the entropy in Fig. 4.

The FP results are based on zero-temperature Fermi-hypernetted-chain correlation functions, with the effective mass as a finite-temperature variational parameter [28]. We note that the density of states at the Fermi surface is underestimated in variational calculations of this type, since the energy dependence of the self energy is properly accounted for only when correlation diagrams are included [29]. In a variational scheme this can be achieved in correlated basis perturbation theory [30,31]. This effect is in part included in the induced interaction, which in neutron matter leads to an enhancement of the effective mass by $\approx 10\%$ (see the RG results for the Fermi liquid parameter $F_1/3 = m^*/m - 1$ in Fig. 6 of Ref. [32]). The enhancement of the effective mass near the Fermi surface is reflected in an increase of the entropy and the specific heat over the variational result at low temperatures [31] (see below).

The pressure P and the entropy per particle S/N are shown in Figs. 3 and 4. As for the free energy, we find a very good agreement with the virial equation of state at low densities, and the inclusion of second-order contributions significantly decreases the cutoff dependence. Our results are similar to the calcu-
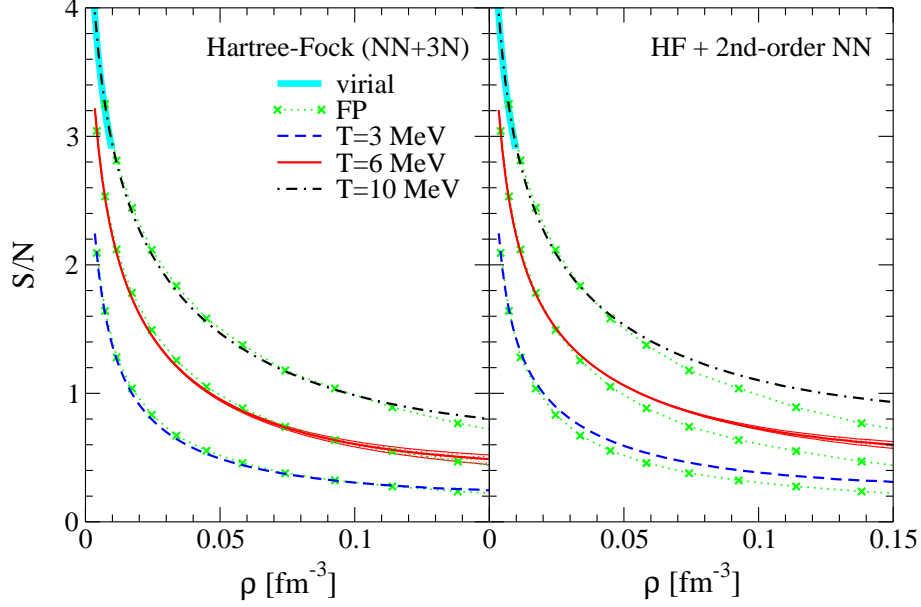
Fig. 4. The entropy per particle S/N as a function of density ρ to first and second order (for details see Fig. 2).
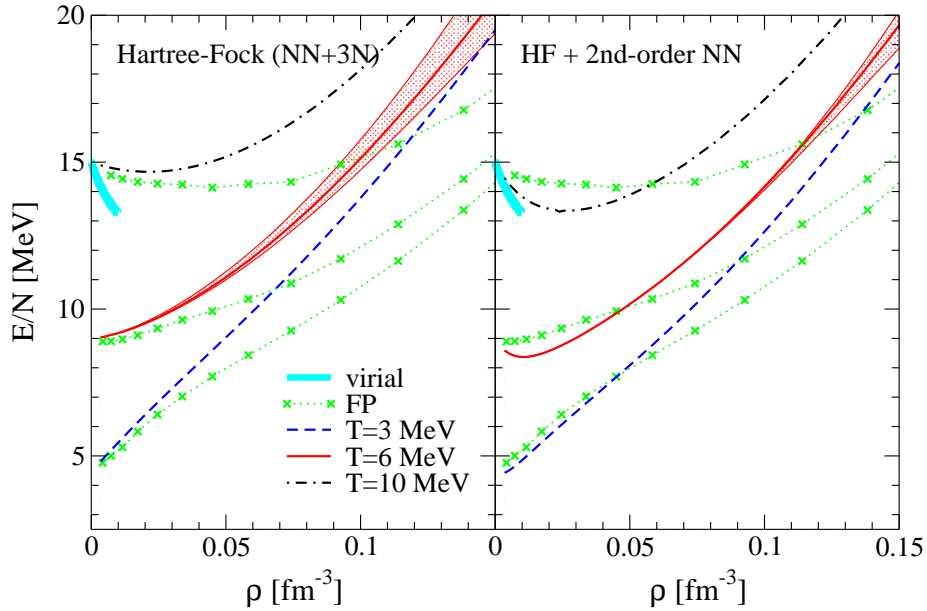

Fig. 5. The energy per particle E/N as a function of density ρ to first and second order (for details see Fig. 2).

lations of FP for densities $\rho \lesssim 0.05 \, \mathrm{fm}^{-3}$. For higher densities, we find a larger pressure and entropy. We emphasize that the results are based on different Hamiltonians, and therefore the comparison has to be taken with care. However, the dominant source for the difference in the entropy is likely due to differences in the effective masses, since the entropy density of a low-temperature Fermi liquid is proportional to the effective mass, $s = m^* k_\mathrm{F} T / 3$ [33]. As discussed above, the variational calculation underestimates the effective mass at
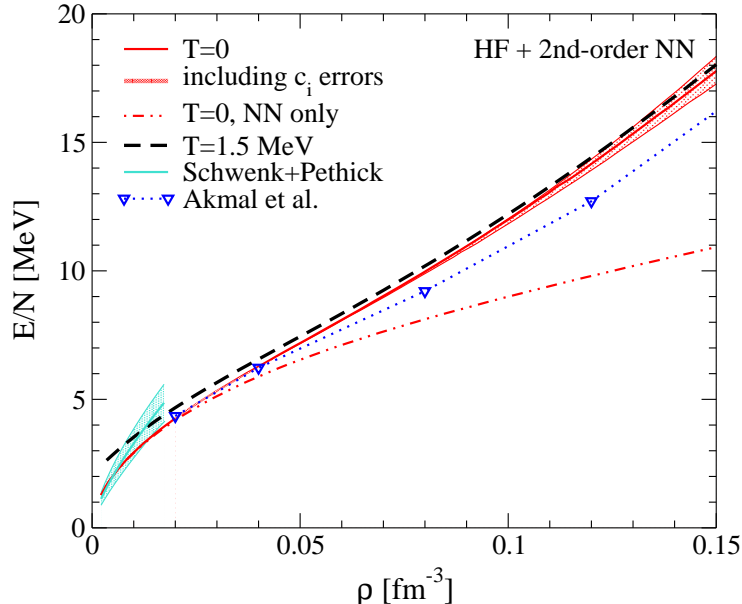
Fig. 6. The energy per particle E/N as a function of density ρ for $T = 0$ and $T = 1.5\,\mathrm{MeV}$. For the $T = 0$ results, we provide error estimates based on the cutoff variation (shaded band) and including the uncertainties in the low-energy constants c_i at this level. The upper and lower limits for the range of c_i values are indicated by the shaded lines. For comparison we also show the model-independent di-fermion EFT results [17] (Schwenk+Pethick) and the results of Akmal *et al.* [35].

the Fermi surface and consequently also the entropy at low temperatures.

Our results for the energy per particle are presented in Fig. 5. As for the free energy, we observe additional binding and a significantly reduced cutoff dependence at second order. In contrast to the variational calculation of FP [22], the low-density behavior at second order is in good agreement with the virial equation of state [21]. This highlights the importance of a correct finite-temperature treatment of second and higher-order contributions. Note that the error in the virial equation of state (due to the neglected third virial coefficient) increases with density. This error is not shown in Fig. 5, but will be discussed in future work on understanding the transition from the perturbative to the virial approach.

A comparison of our low-temperature results to the $T = 0$ energy per particle provides an independent check of our calculations and of the generalized loop expansion. In Fig. 6 we show the energy per particle for $T = 1.5\,\mathrm{MeV}$ for a cutoff $\Lambda = 2.1\,\mathrm{fm}^{-1}$ and the corresponding $T = 0$ equation of state. The latter extends the HF results for neutron matter of Refs. [32,34] to include 3N forces and (normal) second-order NN contributions using an angle-averaged Pauli blocking operator (see Ref. [13] for details). Except at low densities, where $E/N \rightarrow 3/2T$, we find that the $T = 1.5\,\mathrm{MeV}$ energy closely follows the zero temperature results.

In Fig. 6 we provide an error band for the $T = 0$ equation of state based on the cutoff variation. The width of this band is of the same size as for $T = 6\,\text{MeV}$ in Fig. 5. At this level of 3N interactions (leading chiral EFT 3N in HF), only the 2π-exchange part with low-energy constants c_i contribute, and therefore there are no adjustable 3N parameters. Since the c_i constants are cutoff independent, their uncertainties are not fully captured by the cutoff variation, and we therefore directly assess how the presently large uncertainties in c_i propagate to theoretical uncertainties in the neutron matter equation of state at this level. The resulting error estimate in Fig. 6 is based on $c_1 = -0.9^{+0.2}_{-0.5}\,\text{GeV}^{-1}$ and $c_3 = -4.7^{+1.2}_{-1.0}\,\text{GeV}^{-1}$ from Ref. [24]. It is clear that at present the theoretical uncertainties in 3N interactions overwhelm the error due to an approximate many-body treatment for these densities.

We can also compare the $T = 0$ energy per particle at low densities to the the model-independent di-fermion EFT results [17] based directly on the large neutron-neutron scattering length and effective range. Our results are consistent with the di-fermion EFT energy per particle within errors. Finally, the results of Akmal *et al.* [35] (based on the Argonne v_{18} and Urbana IX potential) lie within our error band as well (including the c_i uncertainties). The Urbana IX 3N interaction corresponds to the Δ contribution, $c_3^\Delta = -3.83\,\text{GeV}^{-1}$ [36], and therefore results in less repulsion (with weaker c_3). These results show that, at present, understanding 3N interactions is a frontier for nuclear matter at the extremes.

4 Conclusions

This work is part of a program to improve the nuclear equation of state for astrophysics. One of the central objectives is to quantify the theoretical uncertainties in the microscopic nuclear physics input, and to explore the impact on supernovae and neutron stars, for example, through predictions of neutron star masses and radii.

In this first study of neutron matter, we have computed the equation of state at subsaturation densities and temperatures $T \leqslant 10\,\text{MeV}$ based on low-momentum NN and 3N interactions. We have generalized the perturbative approach [13] to finite temperature, where the free energy is obtained from a loop expansion around the HF energy and the momentum dependence of the self-energy is treated perturbatively. Our results include first-order NN and 3N contributions, as well as anomalous and normal second-order diagrams with NN interactions. The pressure, entropy and energy were then calculated using standard thermodynamic relations. While the HF energy is sizable (and non-perturbative for finite nuclei), the finite-temperature loop expansion around the HF energy seems to be tractable. This is due to a combination of Pauli

blocking [13] and an appreciable effective range [17].

The virial expansion provides a model-independent equation of state for nuclear matter at low density and high temperature [20,21], and our perturbative results meet this benchmark. This is very promising, since it will enable us to match the virial equation of state to microscopic calculations based on NN and 3N interactions at higher densities. The comparison of our results to the virial energy per particle highlights the importance of a correct finite-temperature treatment of second and higher-order correlations, which are included only in an average sense in the variational calculations of Ref. [22]. The correct treatment of thermally-excited low-lying states leads to an enhancement of the effective mass at the Fermi surface and consequently to an increase in the entropy, as shown in Fig. 4.

We have provided simple estimates for the theoretical error by varying the cutoff in low-momentum interactions. This is a powerful tool to assess theoretical errors due to neglected higher-order many-body forces and due to an approximate many-body treatment. We found that the equation of state becomes significantly less cutoff dependent with the inclusion of second-order contributions, and that the cutoff dependence is small for $\rho \lesssim 0.1 \, \text{fm}^{-3}$. We note that the errors of the free energy are correlated between different temperatures and grow with increasing density. The first observation implies a relatively small error in the entropy (obtained by a temperature derivative), and consequently similar errors for the energy per particle. The second observation explains the relatively large error band for the pressure (obtained from a density derivative). Finally, we have shown that the uncertainties due to the long-range parts of 3N interactions, the c_i constants, are substantial and overwhelm the error bands from the cutoff variation at this level. We conclude that understanding 3N forces is a frontier in microscopic calculations of the nuclear equation of state, and furthermore that the possibility of estimating theoretical uncertainties is an important step towards reliable extrapolations to astrophysical conditions.

Future work will include systematic studies of the range of validity, quantifying an expansion parameter for the loop expansion, calculations for asymmetric matter, improving the uncertainties at higher densities, how they propagate to astrophysical observables, and understanding the transition to the virial expansion.

Acknowledgements

References

[1] J.M. Lattimer and M. Prakash, Astrophys. J. **550** (2001) 426.

[2] R. Oechslin, H.T. Janka and A. Marek, Astron. Astrophys. **467** (2007) 395; R. Oechslin and H.T. Janka, Phys. Rev. Lett. **99** (2007) 121102.

[3] A. Mezzacappa, Annu. Rev. Nucl. Part. Sci. **55** (2005) 467.

[4] H.T. Janka, R. Buras, F.S. Kitaura Joyanes, A. Marek and M. Rampp, astro-ph/0405289.

[5] V. Kalogera and G. Baym, Astrophys. J. **470** (1996) 61.

[6] H.A. Bethe, Ann. Rev. Nucl. Sci. **21** (1971) 93.

[7] S.R. Beane, P.F. Bedaque, M.J. Savage and U. van Kolck, Nucl. Phys. **A700** (2002) 377.

[8] S. Fleming, T. Mehen and I.W. Stewart, Nucl. Phys. **A677** (2000) 313.

[9] S.K. Bogner, T.T.S. Kuo and A. Schwenk, Phys. Rept. **386** (2003) 1.

[10] S.K. Bogner, T.T.S. Kuo, A. Schwenk, D.R. Entem and R. Machleidt, Phys. Lett. **B576** (2003) 265.

[11] S.K. Bogner, A. Schwenk, T.T.S. Kuo and G.E. Brown, nucl-th/0111042.

[12] S.K. Bogner, R.J. Furnstahl, S. Ramanan and A. Schwenk, Nucl. Phys. **A784** (2007) 79.

[13] S.K. Bogner, A. Schwenk, R.J. Furnstahl and A. Nogga, Nucl. Phys. **A763** (2005) 59.

[14] S.K. Bogner, R.J. Furnstahl, S. Ramanan and A. Schwenk, Nucl. Phys. **A773** (2006) 203.

[15] A. Nogga, S.K. Bogner and A. Schwenk, Phys. Rev. **C70** (2004) 061002(R).

[16] B.L. Friman, J. Niskanen and E.M. Nyman, Nucl. Phys. **A383** (1982) 285.

[17] A. Schwenk and C.J. Pethick, Phys. Rev. Lett. **95** (2005) 160401.

[18] W. Kohn and J.M. Luttinger, Phys. Rev. **118** (1960) 41.

[19] J.M. Luttinger and J.C. Ward, Phys. Rev. **118** (1960) 1417.

[20] C.J. Horowitz and A. Schwenk, Nucl. Phys. **A776** (2006) 55.

[21] C.J. Horowitz and A. Schwenk, Phys. Lett. **B638** (2006) 153.

[22] B. Friedman and V.R. Pandharipande, Nucl. Phys. **A361** (1981) 502.

[23] M.C.M. Rentmeester, R.G.E. Timmermans and J.J. de Swart, Phys. Rev. **C67** (2003) 044001.

[24] U.-G. Meißner, private communication (2007).

[25] W.H. Press, B.P. Flannery, S.A. Teukolsky and W.T. Vetterling, Numerical Recipes in FORTRAN, Cambridge University Press, 1992.

[26] L. Tolos, B. Friman and A. Schwenk, AIP Conf. Proc. **892** (2007) 508, nucl-th/0611070.

[27] R.B. Wiringa, V.G.J. Stoks and R. Schiavilla, Phys. Rev. **C51** (1995) 38.

[28] I.E. Lagaris and V.R. Pandharipande, Nucl. Phys. **A359** (1981) 331; *ibid.* **A359** (1981) 349.

[29] C. Mahaux, P.F. Bortignon, R.A. Broglia and C.H. Dasso, Phys. Rept. **120** (1985) 1.

[30] S. Fantoni, B.L. Friman and V.R. Pandharipande, Nucl. Phys. **A399** (1981) 51.

[31] S. Fantoni, V.R. Pandharipande and K.E. Schmidt, Phys. Rev. Lett. **48** (1982) 878.

[32] A. Schwenk, B. Friman and G.E. Brown, Nucl. Phys. **A713** (2003) 191.

[33] G. Baym and C.J. Pethick, Landau Fermi Liquid Theory: Concepts and Applications, Wiley, New York, 1991.

[34] A. Schwenk, Int. J. Mod. Phys. **B20** (2006) 2724, nucl-th/0411070.

[35] A. Akmal, V.R. Pandharipande and D.G. Ravenhall, Phys. Rev. **C58** (1998) 1804.

[36] V. Bernard, N. Kaiser and U.-G. Meißner, Nucl. Phys. **A615** (1997) 483.